Measurement and control of turbulence spreading in the Scrape-Off Layer of TJ-II

G. Grenfell[1,2], B.Ph. van Milligen[1], U. Losada[1], W. Ting[1,3], B. Liu[1,4], C. Silva[5], M. Spolaore[2] and C. Hidalgo[1] and the TJ-II Team

[1] National Fusion Laboratory, CIEMAT, Avda. Complutense 40, 28040 Madrid, Spain
[2] Consorzio RFX (CNR, ENEA, INFN, Università di Padova, Acciaierie Venete SpA), C.so Stati Uniti 4, 35127, Padova, Italy
[3] Southwestern Institute of Physics, Chengdu, Sichuan 610041, China
[4] Institute of Fusion Science, School of Physical Science and Technology, Southwest Jiaotong University, 610031 Chengdu, China
[5] Instituto de Plasmas e Fusão Nuclear, Instituto Superior Técnico, Universidade Lisboa, Lisboa, Portugal

Abstract. In this paper, we report measurements of turbulence drive and spreading in the edge region and Scrape-Off Layer (SOL) of the TJ-II stellarator for plasmas heated by ECRH and NBI. In addition, we show how these and various other relevant quantities can be modulated actively via edge biasing, i.e., by establishing an edge flow shear layer. When the edge $E \times B$ shear reaches values close to the inverse of the turbulence correlation time, turbulence spreading and edge-SOL coupling are reduced significantly. The resulting control of SOL spreading via the edge $E \times B$ shear is important in view of the issue of understanding and controlling the SOL width in fusion-relevant devices.

1. Introduction

A critical issue for the development of viable fusion reactors based on magnetic confinement is the power exhaust from the core plasma and the deposition of power on the divertor plates, which may not exceed the thresholds set by material properties. The deposition area and hence the power density is determined to a large extent by the Scrape-Off Layer (SOL) width [1, 2]. Therefore, it is of fundamental importance to dispose of a proper understanding of the mechanisms that set the SOL width, as well as techniques to influence it.

To first order, the SOL width is determined by the competition between cross-field and parallel transport, where parallel transport is typically treated classically, whereas cross-field transport in the SOL is dominated by turbulence [3]. Consequently, it has been suggested that turbulence spreading, i.e., the propagation of turbulence from unstable to stable regions, may play an important role in setting the SOL width [4, 5, 6, 7, 8, 9]. However, reported experimental data on turbulence spreading in the SOL are scarce [10].

In the edge and SOL regions, propagating fluctuations are labelled 'filaments' or 'blobs'. They are coherent structures generated by the nonlinear saturation of turbulence, predominantly traveling outward with a well-defined probability distribution function of the radial velocity [11, 12]. Stochastic models suggesting that the SOL plasma is dominated by traveling filaments [13, 14] have recently been confirmed experimentally [15, 16, 17]. Gyrokinetic simulations indicate that the SOL plasma in ITER might be dominated by blobs and/or streamers [18]. Filaments could be seen as agents of turbulence spreading, carrying the fluctuations from their birth location to other regions. The intermittent behavior of the ion saturation current in different ranges, from the edge to the far SOL, is well characterized in literature [19, 20, 21]. The reports are consistent with the propagation of blobs and holes, lower density fluctuations traveling in the opposite direction to the blobs, and, possibly, with turbulence spreading into the SOL [10].

Turbulent structures with a given size and cross-field velocity can be torn apart by an external $E \times B$ shear, or trapped by it, depend on its strength [22, 23]. Structures born inside the last closed flux surface can be broken into smaller structures or 'blobs' in the SOL [24, 25]. Strong turbulence suppression in the edge can eventually lead to establish of a transport barrier and the improvement of the overall plasma confinement [26]. In tokamaks, the transition from low to high confinement (L-H transition) is characterized by a strong shear layer in the edge; the same is observed in stellarators [27]. Simulations show that filaments and blobs may be involved in the formation of the shear layer [28], which is sometimes preceded by a low-frequency oscillation [29]. The flow shear in the edge can also be achieved or modified with an externally biased electrode that enhances or modifies the radial electric field gradient. This technique has been used to modulate the edge of the plasma both in tokamaks and stellarators [30, 31, 32, 33, 34, 35]. In such experiments, the change in the radial electric field is accessed primarily, before any sharp increase in the pressure profile.

In this paper, we report measurements of the turbulence drive and turbulent spreading in the SOL region of the TJ-II stellarator [36] for plasmas heated by ECRH and NBI, using a recently introduced technique [37]. In addition, we show how these quantities can be controlled by modulating the edge radial electric field during the NBI phase.

2. Experimental setup

TJ-II is a Heliac with toroidal magnetic field $B_T \approx 1$ T, major radius $R_0 = 1.5$ m and minor radius $a < 0.22$ m. The TJ-II heating systems consist of two Electron Cyclotron Resonance Heating (ECRH) sources delivering 300 kW each at a frequency of 53.2 GHz (X mode) and two Neutral Beam Injectors (NBI) producing H co- and counter-beams with up to 2×700 kW port-through power.

The experiments discussed here were performed using the standard magnetic configuration of TJ-II, which has an edge rotational transform close to 1.6 (such that the $n/m = 8/5$ rational surface is located at $\rho \simeq 0.8$). The hydrogen plasmas were heated initially by ECRH and subsequently sustained by NBI heating. The reported results were obtained using NBI co-injection with $P_{\rm NBI} \simeq 500$ kW. Discharges had a line averaged density of about $\overline{n}_e = 1 \times 10^{19}$ m^{-3} and central electron temperatures in the range of $300 < T_e(0) < 400$ eV. All experiments were carried out in a single day to ensure optimal reproducibility.

A 2-D Langmuir probe array Fig. 1 was used to measure the floating potential (ϕ_f) and the ion saturation current (I_s). 5×4 pins of the probe are arranged in a grid such that 4 tips in a row are aligned poloidally with a mutual distance of 3 mm and 5 tips in a column are aligned radially with a mutual distance of 5 mm. Signals were sampled at a rate of 2 MHz. Turbulent particle transport is calculated as $\Gamma_r \simeq \langle \tilde{n}_e \tilde{v}_r \rangle \propto \langle \tilde{I}_s \tilde{E}_\theta \rangle / B$, neglecting electron temperature fluctuations, where the angular brackets indicate a temporal average and $\tilde{E}_\theta \approx -\Delta\tilde{\phi}_f/\Delta\theta$. Electrostatic fluctuations produce a fluctuating radial velocity given by $\tilde{v}_r = \tilde{E}_\theta / B$, where $\tilde{E}_\theta$ is the fluctuating poloidal electric field and B the toroidal magnetic field. We define an effective mean radial velocity by normalizing the turbulent $E \times B$ particle transport to the local density: $v_r^{\rm eff} = \langle \tilde{I}_s \tilde{E}_\theta \rangle / I_s B$. This effective velocity is not affected by uncertainties in the probe area, thus providing a convenient way to investigate the statistical properties of the radial propagation of fluctuations in the SOL region. The phase velocity of the fluctuations (perpendicular to both the magnetic field and the poloidal direction) was computed using the two-point correlation technique [38] from two poloidally separated floating potential signals.

The probe was moved from the far SOL into the deep edge on a shot by shot basis. Global parameters were kept approximately constant; an example is shown in Fig. 2. NBI injection provokes a notable change in the plasma parameters, increasing the average central line density from $\overline{n}_e \simeq 0.6 \times 10^{19}$ m^{-3} in the ECRH phase to around 0.9×10^{19} m^{-3} in the NBI phase. Away from the short ECRH to NBI transition phase,

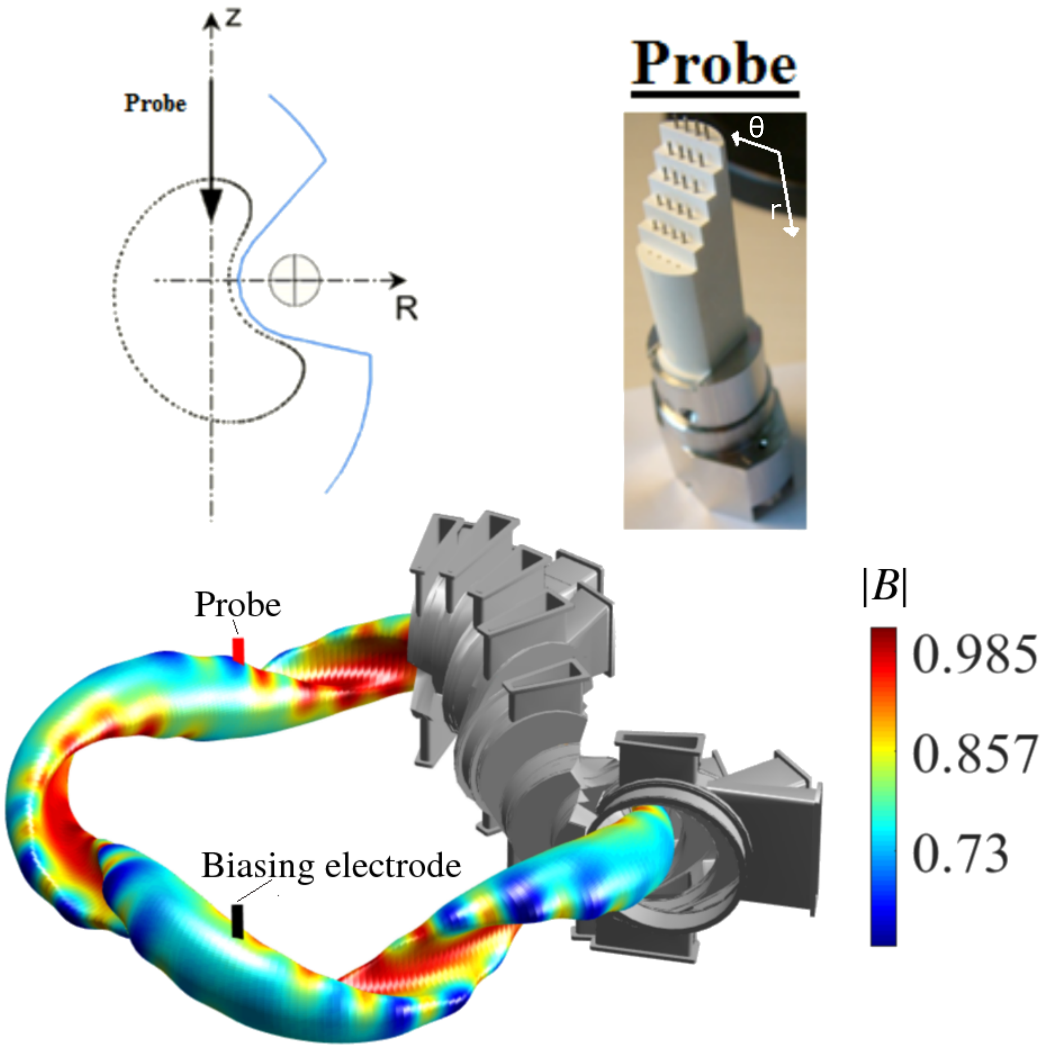

Figure 1. Schematic diagram of the 2-D probe: top left, a cross section at $\phi = 38.2°$ showing the plasma (black dotted line) and the vacuum vessel (blue line) as well as the probe trajectory, inserted vertically from the top; bottom: 3-D graph showing the last closed flux surface, colored in accordance with the magnetic field strength $|B|$, and the insertion points of the 2-D probe (red) and the biasing probe (black), as well as the vacuum chamber of one of the four sections of TJ-II. Top right: a photo of the 2-D probe.

the plasma regime is roughly stationary. The edge radial electric field was modified by means of a biasing electrode inserted into the edge of the plasma (insertion point: $\rho \simeq 0.85$ [39] ($\rho = \sqrt{\psi_N}$, where ψ_N is the normalized magnetic flux, $\psi_N = \psi/\psi_{\rm LCFS}$, and $\psi_{\rm LCFS}$ is the value of the flux at the Last Closed Flux Surface). The electrode is made of mushroom-shaped graphite, 25 mm diameter and 12 mm height, inserted in a boron nitride insulating body. At TJ-II, external biasing is capable of controlling the edge plasma potential fully. The concomitant density rise has been attributed unequivocally to an improvement in particle confinement [40]. The imposed field affects the strength of the edge $E_r \times B$ shear layer, allowing us to study the impact of edge biasing on the behavior of turbulence spreading and plasma profiles. The applied biasing was a 40 Hz square signal with an amplitude of -350 V and a duty cycle of 50% .

3. Data analysis

To study turbulence drive and spreading, we make use of the technique introduced in Ref. [37]. According to this work, one can obtain the time evolution of free turbulent energy $\langle \tilde{n}^2 \rangle$ (where $\tilde{n} = n - \langle n \rangle$) to good approximation from the radial part of the continuity equation by neglecting cross-field coupling and damping as well as the effect of background flows (i.e., $\langle v_r \rangle = 0$) and considering incompressible turbulence in the

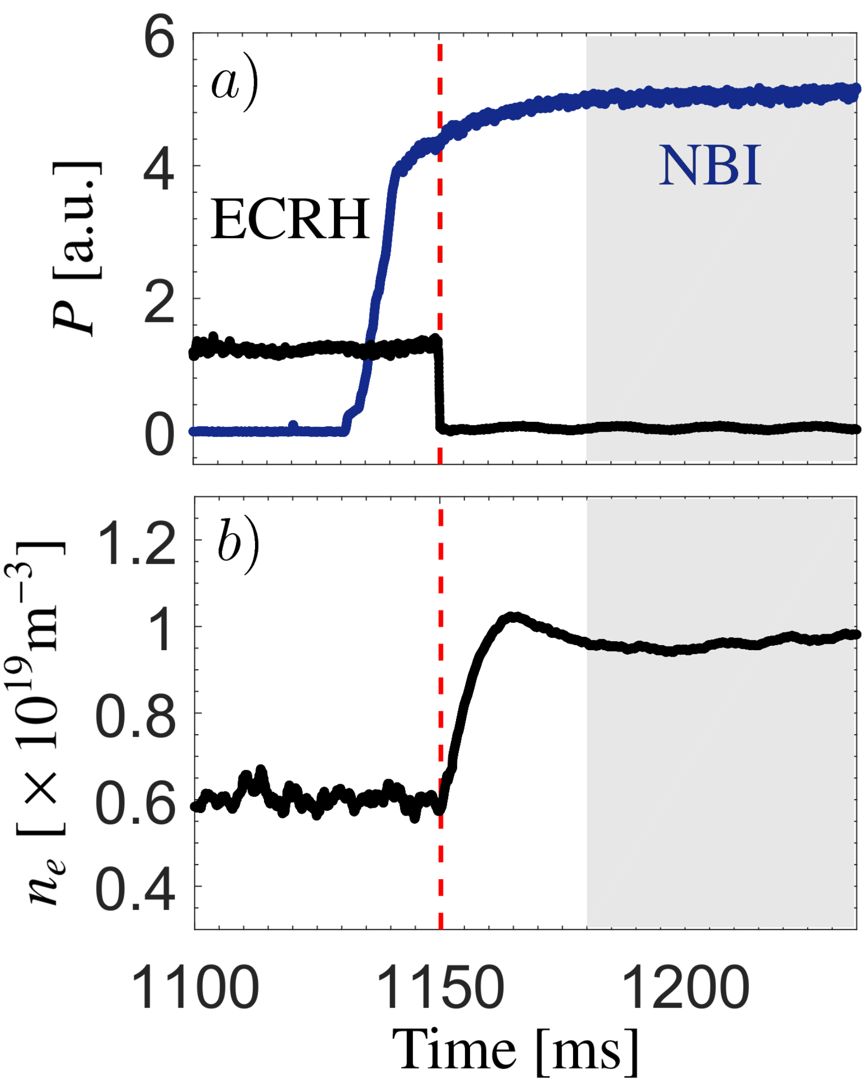

Figure 2. Plasma parameters during the transition from ECRH to NBI plasmas in the TJ-II; a) heating power in arbitrary units and b) line averaged density. The grey area indicates the time window where biasing was applied.

plane perpendicular to the magnetic field. The angular brackets $\langle ... \rangle$ indicate a running average over a time interval much larger than the turbulence correlation time (see below). With these approximations, the evolution of turbulent energy is given by:

$$\frac{1}{2}\frac{\partial}{\partial t}\langle \tilde{n}^2 \rangle = -\langle \frac{\partial n}{\partial r} \rangle \langle \tilde{v}_r \tilde{n} \rangle - \frac{1}{2}\frac{\partial}{\partial r}\langle \tilde{v}_r \tilde{n}^2 \rangle \tag{1}$$

The first term RHS of Eq. 1 is related to the local drive of turbulence by the background (gradient), while the second term is a nonlocal nonlinear term related to turbulence spreading. Through normalization by the local turbulence amplitude, $\langle \tilde{n}^2 \rangle$, one defines the rate of turbulence drive:

$$\omega_D = -\frac{2\langle \frac{\partial n}{\partial r} \rangle \langle \tilde{v}_r \tilde{n} \rangle}{\langle \tilde{n}^2 \rangle} \tag{2}$$

and the rate of turbulence spreading:

$$\omega_S = -\frac{\frac{\partial}{\partial r}\langle \tilde{v}_r \tilde{n}^2 \rangle}{\langle \tilde{n}^2 \rangle} \tag{3}$$

Our probe setup allowed us to compute both quantities, assuming $n \propto I_s$ and $E_\theta \simeq -\Delta\phi_f/d$, where d is the poloidal distance between the two corresponding floating potential probe pins. Therefore, neglecting electron temperature fluctuations, one obtains $\omega_D \simeq -2\langle \partial I_s/\partial r \rangle \langle \tilde{E}_\theta \tilde{I}_s \rangle / (B_T \langle \tilde{I}_s^2 \rangle)$ and $\omega_S = -\partial/\partial r \langle \tilde{E}_\theta \tilde{I}_s^2 \rangle / (B_T \langle \tilde{I}_s^2 \rangle)$. In order to measure these parameters, we use two rows of pins, such that each row has 1 pin measuring the ion saturation current, placed between two pins each measuring the floating potential. The angular brackets $\langle ... \rangle$ here mean a running average over a time interval of 1 (or 2) ms.

4. Experimental results

4.1. Transition from ECRH to NBI

During the transition from ECRH to NBI, the profile of the radial electric field changes strongly. The switch to NBI leads to an increase of density, which causes a global sign change of the plasma potential [41] and confinement changes from electron root to ion root [42]. Namely, the Neoclassical radial electric field profile corresponds to different solutions of the line average density [43], which has an impact on the edge $E \times B$ shear flow layer.

Fig. 3 shows the evolution of the floating potential (ϕ_f), ion saturation current (I_s), radial turbulent particle flux (Γ_r) and phase velocity of the fluctuations in the poloidal direction (v_θ^{ph}) during the transition from ECRH to NBI. The shown results were calculated as averages over 2 ms time windows. Turbulent fluctuations here and in the following were band-pass filtered in the range $(5 - 700)$ kHz. The transition from the electron to the ion root is clearly seen in the ϕ_f signal: the floating potential is initially nearly flat in the ECRH phase, but becomes rather steep during NBI, with a high gradient close to the edge. This change is accompanied by the establishment of a poloidal velocity shear layer, clearly seen in Fig. 3 d) near $r - r_0 \simeq -15$ mm. As

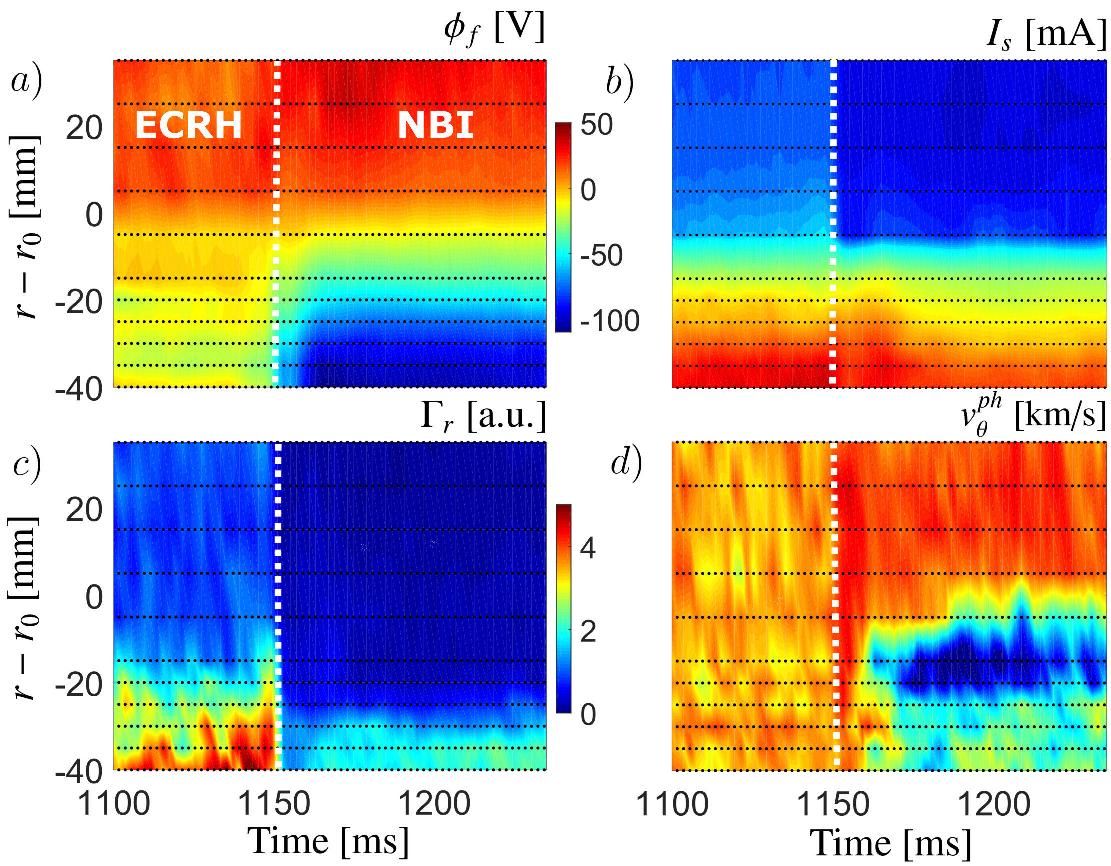

Figure 3. Plasma parameters during the transition from ECRH to NBI; a) the radial profile of floating potential, b) ion saturation current, c) turbulent particle flux and d) turbulence phase velocity in the TJ-II plasma boundary region. The vertical axis shows the radial position (r) relative to the the location of the Last Closed Flux Surface (LCFS, r_0). Negative values of $r - r_0$ correspond to the plasma edge, positive values to the SOL. The horizontal black lines indicate the locations of probe pins.

consequence, the turbulent particle flux is greatly modified Fig. 3 c) and drops sharply in the NBI phase where the shear layer is presented. The ion saturation current, related to the electron density and temperature via $I_s \propto n_e T_e^{-1/2}$, is also strongly affected during NBI, exhibiting a slight decrease in the edge and a strong reduction in the SOL.

To summarize these results and facilitate their understanding, Fig. 4 displays time averages of these and a few other quantities. The curves labelled ECRH were calculated over $1100 < t < 1140$ ms, while those labelled NBI were calculated over $1180 < t < 1220$ ms. As noted, the edge profiles of ϕ_f and I_s are less pronounced in ECRH than in NBI, and the base level of I_s is higher in the SOL Fig. 4 b), i.e., it has a longer 'tail' that extends to the far SOL. Similarly, Γ_r is flatter and much higher during ECRH in the SOL. As noted before, during NBI a shear layer develops near the edge at $r - r_0 \simeq -15$ mm, clearly visible in the graph of $v_\theta^{\rm ph}$ Fig. 4 f). The maximum shear in the poloidal phase velocity (dv_θ/dr) during NBI is $4 \cdot 10^5$ s^{-1}, while during ECRH it is $0.3 \cdot 10^5$ s^{-1} at the same position. The evolution of the phase velocity (v_θ^{ph}) can be explained in

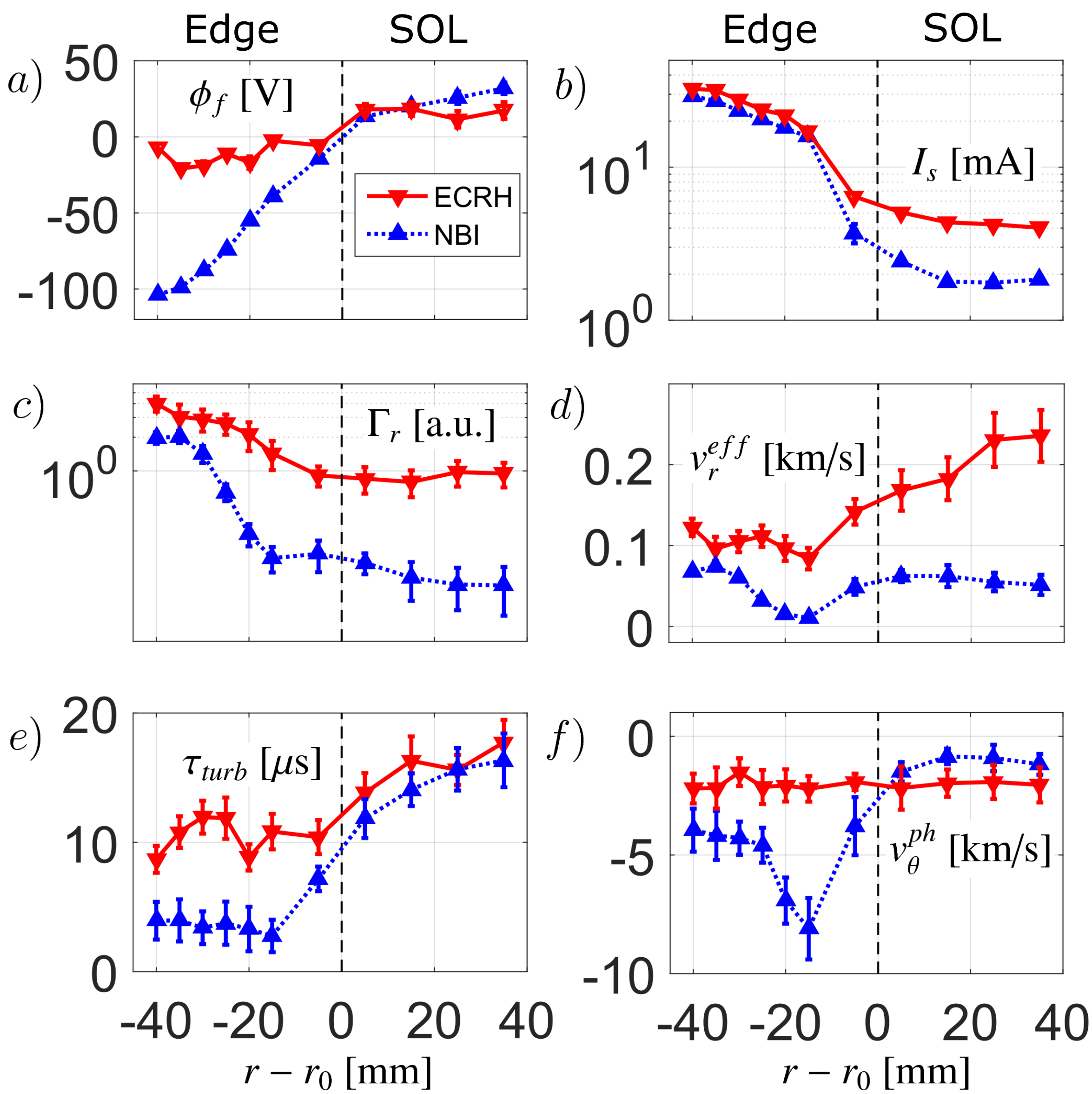

Figure 4. Radial profiles of (a) floating potential, (b) ion saturation current, (c) turbulent transport, (d) radial effective velocity, (e) turbulence correlation time and (f) phase velocity of the fluctuations during plasma heated by ECRH and NBI.

terms of $E \times B$ drift [44], in agreement with previous results [45, 46]. This remarkable difference has a strong impact on the radial turbulent particle flux shown in Fig. 4 c). The strong shear is likely related to the reduction of the turbulence correlation time (τ_{turb} - from the auto-correlation of the floating potential) in the edge Fig. 4 e) and the reduction of the effective radial turbulent velocity (v_r^{eff}) in the edge and SOL Fig. 4 d). In conclusion, the spontaneous establishment of the edge poloidal velocity shear layer affects all indicators of turbulent transport and has a significant impact not only at the location of the shear layer itself (in the edge, close to the LCFS), but also further outward (the SOL).

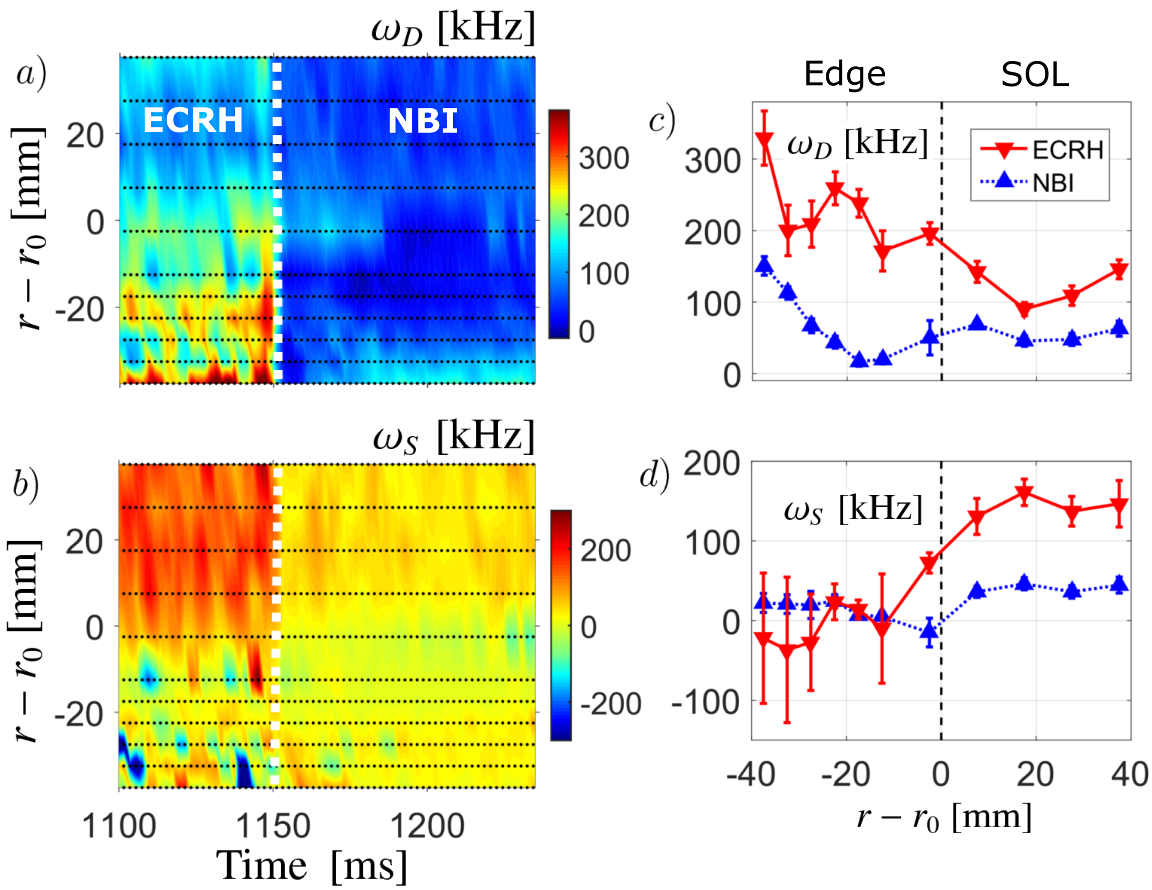

Figure 5. The effect of the transition from ECRH to NBI plasma heating on the local turbulence drive a) and c) (ω_D) and the turbulence spreading b) and d) (ω_S). The horizontal black lines indicate the locations of probe pins.

To shed more light on the radial propagation of these effects, we computed the turbulence drive (ω_D) and spreading (ω_S) (Fig. 5). These parameters were evaluated by calculating the moving average and RMS values of the ion saturation current and floating potential from the two innermost rows of probe pins.

The figure suggests that the high base line of the turbulent particle flux in the SOL in the ECRH phase is related to both the turbulence drive and spreading, as both parameters have comparable values in this range. The local linear growth term is high in the edge and lower in the SOL, consistent with the variation of the density gradient (high in the edge and low in the SOL) during ECRH. In the NBI phase, ω_D drops more strongly in the edge region (particularly at the location of the poloidal velocity shear layer) than in the SOL. On the other hand, the turbulence spreading rate (ω_S) is higher in the SOL than in the edge (especially in the ECRH heating phase), while its value is comparable to the local linear growth rate (ω_D) in this range in both heating regimes.

4.2. NBI + biasing

The influence of edge biasing on various plasma profiles is shown in Fig. 6. Twelve reproducible shots were used to measure the profiles of floating potential (ϕ_f), ion saturation current (I_s), radial turbulent particle flux (Γ_r), effective radial velocity (v_r^{eff}), turbulence correlation time (τ_{turb}) and phase velocity of the fluctuations in the poloidal direction (v_θ^{ph}) during dynamical edge biasing in the NBI phase.

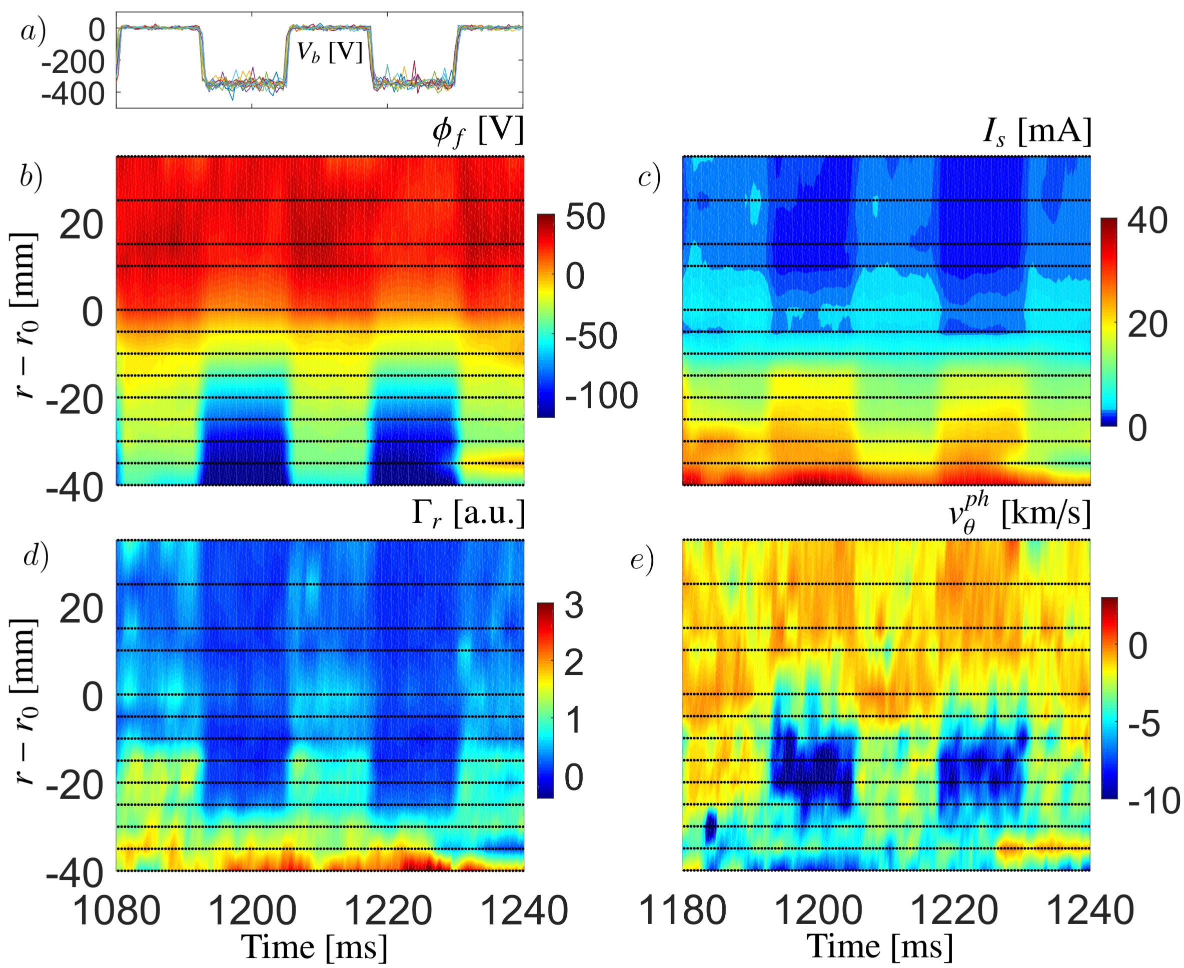

Figure 6. a) Biasing voltage and its effect on b) the radial profile of floating potential, c) ion saturation current, d) turbulent particle flux and e) turbulence phase velocity in the TJ-II plasma boundary region. The vertical axis shows the radial position (r) relative to the the location of the Last Closed Flux Surface (LCFS, r_0). Negative values of $r - r_0$ correspond to the plasma edge, positive values to the SOL. The horizontal black lines indicate the locations of probe pins.

Fig. 6 shows the modulation of b) the floating potential, c) the ion saturation current and d) the turbulent particle flux (Γ_r) in time. The analyses were performed in time sections with a length of 1 ms. The fast rise and fall of the biasing voltage (Fig. 6a) provokes a fast readjustment of the profiles, which are affected most inside the LCFS.

These results are again summarized in Fig. 7, which shows averages over the biasing on/off phases. During the negative biasing phases (-350 V), the floating potential profiles (Fig. 7a) and edge ion saturation current (Fig. 7b) steepen in the plasma edge region while the turbulent particle flux (Fig. 7c) and effective radial turbulence velocity (Fig. 7d) are reduced in both edge and SOL ($r - r_0 > -30$ mm), concomitant with a reduction in the magnitude of the ion saturation current in the SOL.

The phase velocity of the fluctuations $v_\theta^{\rm ph}$ is shown in (Fig. 7f). During the negative biasing phase, the plasma edge potential becomes more negative, the radial gradient in floating potential profiles reaches values up to -7.9 kV/m ($v_\theta = E_r/B \approx -\Delta\phi_f/\Delta rB$, where $B \approx 1$ T) and the perpendicular velocity increases up to -9 km/s, showing that the

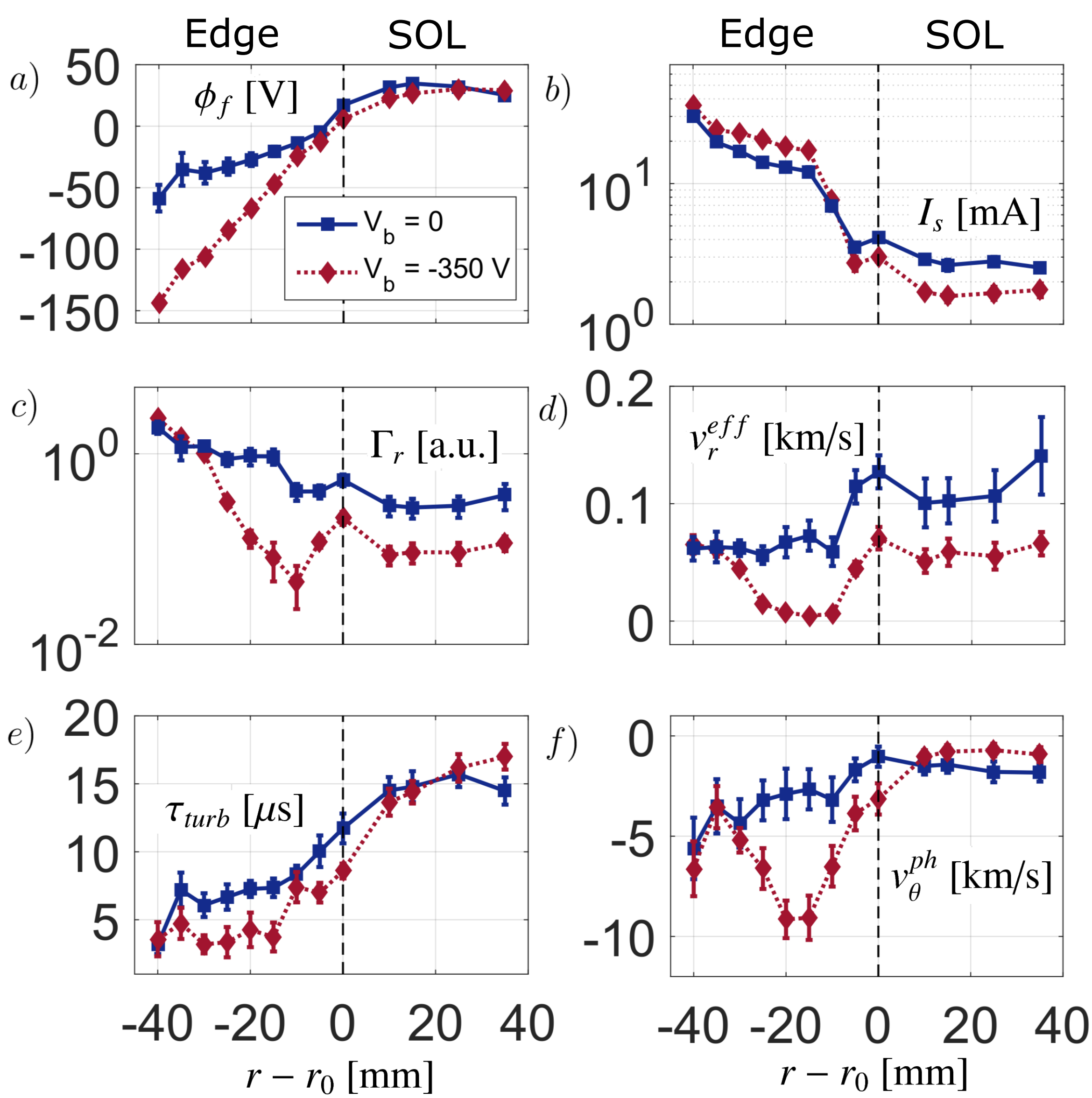

Figure 7. Radial profiles of (a) floating potential, (b) ion saturation current, (c) turbulent transport, (d) radial effective velocity, (e) turbulence correlation time and (f) phase velocity of the fluctuations during biasing 0 V and -350 V.

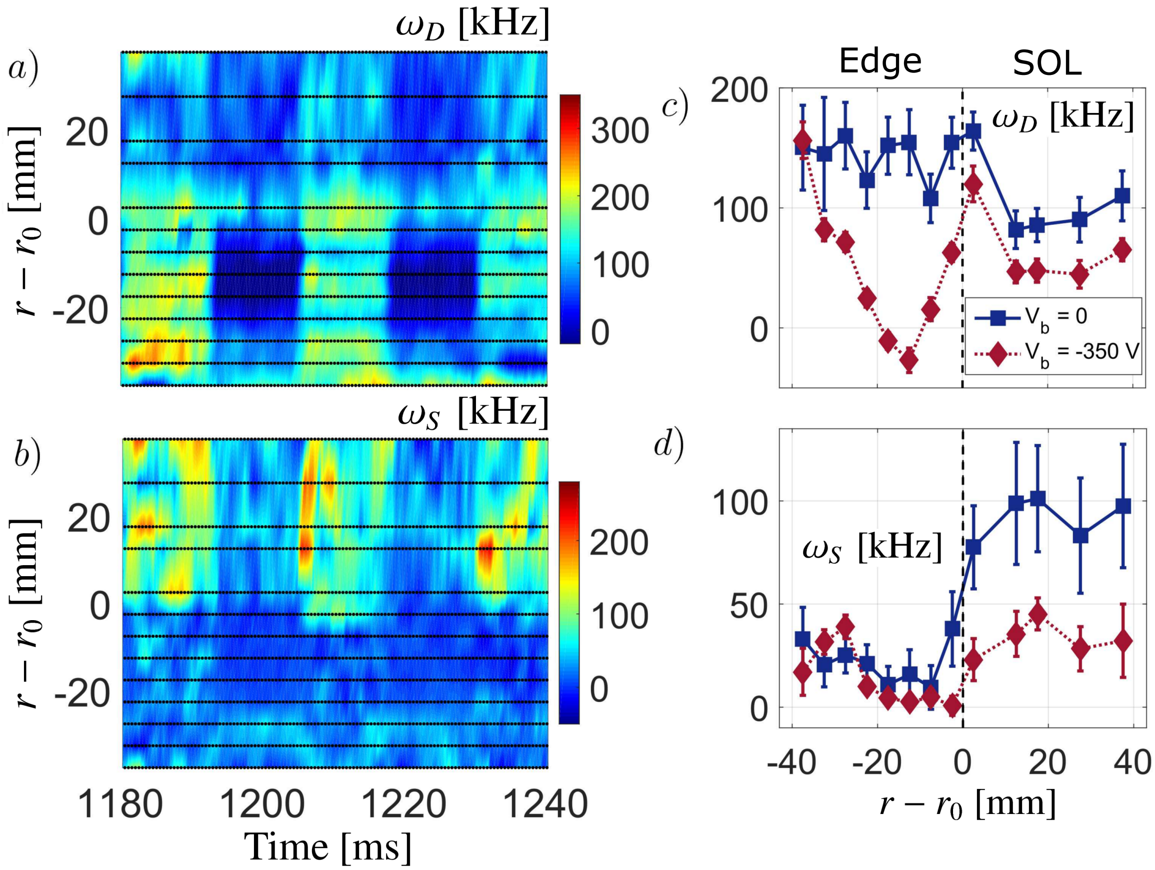

Figure 8. The impact of edge biasing on the local turbulence drive a) and c) (ω_D) and the turbulence spreading b) and d) (ω_S). The horizontal black lines indicate the locations of probe pins.

measured phase velocity is mainly due to the imposed $E_r \times B$ drift [47]. The maximum shear in the perpendicular velocity (dv_θ/dr) is of the order of $5 \cdot 10^5$ s^{-1}, i.e., close to the inverse of the turbulence decorrelation time (Fig. 7e) [48]. The maximum shear occurs near $r - r_0 \simeq -10$ mm. This result is in agreement with, e.g., conclusions reported at the LAPD device [49], where limiter biasing was shown to control the turbulent particle flux, dropping to values near zero when the shearing rates became comparable to the inverse of correlation time at zero shearing.

In view of the previous results, we conclude that the enhancement of the velocity shear at -350 V biasing (Fig. 7f) leads to the reduction of the base level of the ion saturation current in the SOL (Fig. 7b), the amplitude of turbulent transport (Fig. 7c) and the effective radial velocity of fluctuations in the SOL region (Fig. 7d). Thus, the increase in $E_r \times B$ shear in the vicinity of the LCFS has a strong impact on SOL density (I_s), and turbulent transport profiles.

The impact of edge biasing on the local turbulence drive (ω_D) and turbulence spreading (ω_S) is shown in Fig. 8. At 0 V biasing, the local growth rate term (ω_D) is high in the edge and low in the SOL, roughly consistent with the variation of the density gradient (high in the edge and low in the SOL, Fig. 7b). At -350 V biasing, ω_D is strongly suppressed at the shear layer position, cf. Fig. 7f), consistent with the idea of turbulence suppression by the $E \times B$ sheared flow. On the other hand, the rate of turbulence spreading (ω_S) is much higher in the SOL than in the edge at 0 V biasing, where its amplitude is comparable to the local growth rate, while it is reduced at -350 V biasing, more strongly in the SOL region Figs. 7b) and d).

It seems that the velocity shear layer that forms in the edge region at negative biasing (Fig. 7f) constitutes a transport barrier that partially decouples the edge and SOL regions [50, 51], both by suppressing edge turbulence (local turbulence drive - ω_D) and by reducing outward turbulent transport (spreading - ω_S) [21]. A similar effect, though less intense, is observed during the transition from ECRH to NBI Fig. 4 and Fig. 5. One would expect such a decoupling to lead to a reduction of the SOL width (the SOL density scale length), assuming parallel transport remains constant. Indeed, this seems to be consistent with the I_s curves shown in Fig. 7b).

5. Conclusions

In this paper, we report experimental measurements of the turbulence drive and turbulent spreading in the SOL region of the TJ-II stellarator. The experimental data are consistent with the results obtained from a three dimensional gyro fluid turbulence model [37], in which spreading is also shown to be mainly active in the SOL region. This effect was demonstrated for plasma heated by both ECRH and NBI. For the latter, the effect is less pronounced due to a strong shear close to the LCFS, which reduces the local turbulence and the spreading in the SOL. Besides, we show, for the first time, how the turbulence drive and spreading terms can be modulated via edge biasing and the generation of a velocity shear layer in the edge, with possible consequences for the SOL width. When the $E_r \times B$ shear reaches values close to the inverse of the turbulence correlation time in the vicinity of the LCFS, edge-SOL coupling is reduced significantly [52] as well as turbulence spreading. The observed relation between the edge shear layer and turbulence in the SOL is relevant both for tokamaks and stellarators when edge shear flows are established near the LCFS.

Consequently, we find that the edge radial electric field shear is an important tool for suppressing turbulence, decoupling the edge and SOL regions and reducing non-local effects (spreading). As turbulent drive and spreading are likely important factors in setting the SOL width, together with parallel dynamics, we believe the approach reported here provides a route to a better understanding of power exhaust in fusion plasmas.

6. Acknowledgements

The authors acknowledge useful discussions with P. Manz. Research sponsored in part by the Ministerio de Economía y Competitividad of Spain under project

Nr. ENE2015-68206-P. This work has been carried out within the framework of the EUROfusion Consortium and has received funding from the Euratom research and training programme 2014-2018 under grant agreement No 633053 and from Erasmus Mundus International Doctoral College in Fusion Science and Engineering (FUSION-DC). The views and opinions expressed herein do not necessarily reflect those of the European Commission.

References

[1] T. Eich, B. Sieglin, A. Scarabosio, W. Fundamenski, R.J. Goldston, and A. Herrmann. Inter-ELM power decay length for JET and ASDEX upgrade: measurement and comparison with heuristic drift-based model. *Phys. Rev. Lett.*, 107(21):215001, 2011.

[2] J. Horacek, R. A. Pitts, J. Adamek, G. Arnoux, J.-G. Bak, S. Brezinsek, M. Dimitrova, R. J. Goldston, J. P. Gunn, J. Havlicek, S.-H. Hong, F. Janky, B. LaBombard, S. Marsen, G. Maddaluno, L. Nie, V. Pericoli, Tsv Popov, R. Panek, D. Rudakov, J. Seidl, D. S. Seo, M. Shimada, C. Silva, P. C. Stangeby, B. Viola, P. Vondracek, H. Wang, G. S. Xu, Y. Xu, and JET Contributors. Multi-machine scaling of the main SOL parallel heat flux width in tokamak limiter plasmas. *Plasma Phys. Control. Fusion*, 58:074005, 2016.

[3] J.R. Myra, D.A. Russell, D.A. D'Ippolito, J-W. Ahn, R. Maingi, R.J. Maqueda, D.P. Lundberg, D.P. Stotler, S.J. Zweben, and M.Umansky. Turbulent transport and the scrape-off-layer width. *J. Nucl. Mat.*, 415(1):S605, 2011.

[4] N. Mattor and P.H. Diamond. Drift wave propagation as a source of plasma edge turbulence. *Phys. Rev. Lett.*, 72(4):486, 1994.

[5] X. Garbet, L. Laurent, A. Samain, and J. Chinardet. Radial propagation of turbulence in tokamaks. *Nucl. Fusion*, 34(7):963, 1994.

[6] Ö.D. Gürcan, P.H. Diamond, T.S. Hahm, and Z. Lin. Dynamics of turbulence spreading in magnetically confined plasmas. *Phys. Plasmas*, 12(3):032303, 2005.

[7] W.X. Wang, T.S. Hahm, W.W. Lee, G. Rewoldt, J. Manickam, and W.M. Tang. Nonlocal properties of gyrokinetic turbulence and the role of E× B flow shear. *Phys. Plasmas*, 14(7):072306, 2007.

[8] L. Isoardi, G. Ciraolo, G. Chiavassa, P. Haldenwang, E. Serre, Ph. Ghendrih, Y. Sarazin, F. Schwander, X. Garbet, and P. Tamain. Modelling SOL flow pattern spreading in the edge plasma. *J. Nucl. Mat.*, 390-391:388, 2009.

[9] T. Estrada, C. Hidalgo, and T. Happel. Signatures of turbulence spreading during the H-L back-transition in TJ-II plasmas. *Nucl. Fusion*, 51(3):032001, 2011.

[10] O. Pan, Y. Xu, J. Cheng, J.Q. Xu, L.W. Yan, K. Yao, M. Xu, Z.B. Shi, Yi Liu, Q.W. Yang, X.R. Duan, Y. Liu, and the HL-2A team. Investigation of mechanisms for the generation of blobs/holes at the boundary of the HL-2A tokamak. In *Proc. 26*$^{\text{th}}$ *IAEA Fusion Energy Conference (Kyoto, Japan)*, pages EX/P7–29, 2016.

[11] G.Q. Yu and S.I. Krasheninnikov. Dynamics of blobs in scrape-off-layer/shadow regions of tokamaks and linear devices. *Phys. Plasmas*, 10(11):4413–4418, 2003.

[12] D.A. DIppolito, J.R. Myra, and S.J. Zweben. Convective transport by intermittent blob-filaments: Comparison of theory and experiment. *Phys. Plasmas*, 18(6):060501, 2011.

[13] O.E. Garcia, R. Kube, A. Theodorsen, and H.L. Pécseli. Stochastic modelling of intermittent fluctuations in the scrape-off layer: Correlations, distributions, level crossings, and moment estimation. *Phys. Plasmas*, 23(5):052308, 2016.

[14] F. Militello and J.T. Omotani. Scrape off layer profiles interpreted with filament dynamics. *Nucl. Fusion*, 56(10):104004, 2016.

[15] N.R. Walkden, A. Wynn, F. Militello, B. Lipschultz, G. Matthews, C. Guillemaut, J. Harrison, D. Moulton, and JET Contributors. Interpretation of scrape-off layer profile evolution and

first-wall ion flux statistics on JET using a stochastic framework based on fillamentary motion. *Plasma Phys. Control. Fusion*, 59(8):085009, 2017.

[16] R. Kube, A. Theodorsen, O.E. Garcia, B. LaBombard, and J.L. Terry. Fluctuation statistics in the scrape-off layer of Alcator C-Mod. *Plasma Phys. Control. Fusion*, 58(5):054001, 2016.

[17] R. Kube, O.E. Garcia, A. Theodorsen, D. Brunner, A.Q. Kuang, B. LaBombard, and J.L. Terry. Intermittent electron density and temperature fluctuations and associated fluxes in the Alcator C-Mod scrape-off layer. *Plasma Phys. Control. Fusion*, 60(6):065002, 2018.

[18] C.S. Chang, S. Ku, A. Loarte, V. Parail, F. Kchl, M. Romanelli, R. Maingi, J.-W. Ahn, T. Gray, J. Hughes, B. LaBombard, T. Leonard, M. Makowski, and J. Terry. Gyrokinetic projection of the divertor heat-flux width from present tokamaks to ITER. *Nucl. Fusion*, 57(11):116023, 2017.

[19] J.A. Boedo, D. Rudakov, R. Moyer, S. Krasheninnikov, D. Whyte, G. McKee, G. Tynan, M. Schaffer, P. Stangeby, P. West, et al. Transport by intermittent convection in the boundary of the DIII-D tokamak. *Phys. Plasmas*, 8(11):4826–4833, 2001.

[20] J. Cheng, L.W. Yan, W.Y. Hong, K.J. Zhao, T. Lan, J. Qian, A.D. Liu, H.L. Zhao, Yi. Liu, Q.W. Yang, et al. Statistical characterization of blob turbulence across the separatrix in HL-2A tokamak. *Plasma Phys. Control. Fusion*, 52(5):055003, 2010.

[21] G.S. Xu, V. Naulin, W. Fundamenski, C. Hidalgo, J.A. Alonso, C. Silva, B. Gonçalves, A. H. Nielsen, J. Juul Rasmussen, S.I. Krasheninnikov, B.N. Wan, M. Stamp, and JET EFDA Contributors. Blob/hole formation and zonal-flow generation in the edge plasma of the JET tokamak. *Nucl. Fusion*, 49(9):092002, 2009.

[22] Nirmal Bisai, Amita Das, Shishir Deshpande, Ratneshwar Jha, Predhiman Kaw, Abhijit Sen, and Raghvendra Singh. Edge and scrape-off layer tokamak plasma turbulence simulation using two-field fluid model. *Phys. Plasmas*, 12(7):072520, 2005.

[23] M. Agostini, S.J. Zweben, R. Cavazzana, P. Scarin, G. Serianni, R.J. Maqueda, and D.P. Stotler. Study of statistical properties of edge turbulence in the National Spherical Torus Experiment with the gas puff imaging diagnostic. *Phys. Plasmas*, 14(10):102305, 2007.

[24] G. Fuchert, G. Birkenmeier, B. Nold, M. Ramisch, and U. Stroth. The influence of plasma edge dynamics on blob properties in the stellarator TJ-K. *Plasma Phys. Control. Fusion*, 55(12):125002, 2013.

[25] B. Nold, P. Manz, T.T. Ribeiro, G. Fuchert, G. Birkenmeier, H.W. Müller, M. Ramisch, B.D. Scott, and U. Stroth. Turbulent transport across shear layers in magnetically confined plasmas. *Phys. Plasmas*, 21(10):102304, 2014.

[26] P.H. Diamond, S-I Itoh, K. Itoh, and T.S. Hahm. Zonal flows in plasma-a review. *Plasma Phys. Control. Fusion*, 47(5):R35, 2005.

[27] F. Wagner. A quarter-century of H-mode studies. *Plasma Phys. Control. Fusion*, 49(12 B):B1, 2007.

[28] J.R. Myra, W.M. Davis, D.A. D'Ippolito, B. LaBombard, D.A. Russell, J.L. Terry, and S.J. Zweben. Edge sheared flows and the dynamics of blob-filaments. *Nucl. Fusion*, 53(7):073013, 2013.

[29] S.J. Zweben, R.J. Maqueda, R. Hager, K. Hallatschek, S.M. Kaye, T. Munsat, F.M. Poli, A.L. Roquemore, Y. Sechrest, and D.P. Stotler. Quiet periods in edge turbulence preceding the LH transition in the National Spherical Torus Experiment. *Phys. Plasmas*, 17(10):102502, 2010.

[30] R. J. Taylor, M. L. Brown, B. D. Fried, H. Grote, J. R. Liberati, G. J. Morales, P. Pribyl, D. Darrow, and M. Ono. H-mode behavior induced by cross-field currents in a tokamak. *Phys. Rev. Lett.*, 63(21):2365–2368, 1989.

[31] R. R. Weynants, G. van Oost, G. Bertschinger, J. Boedo, P. Brys, T. Delvigne, K.H. Dippel, F. Durodie, H. Euringer, K.H. Finken, D.S. Gray, J.D. Hey, D.L. Hillis, J.T. Hogan, L. Konen, R. Leners, A.M. Messiaen, A. Pospieszczyck, U. Samm, R.P. Schorn, B. Schweer, G. Telesca, R. van Nieuwenhove, and P.E. Vandenplas. Confinement and profile changes induced by the presence of positive or negative radial electric fields in the edge of the TEXTOR tokamak. *Nucl.*

Fusion, 32(5):837, 1992.

[32] C. Hidalgo, M.A. Pedrosa, N. Dreval, K.J. McCarthy, L. Eliseev, M.A. Ochando, T. Estrada, I. Pastor, E. Ascasíbar, E. Calderón, et al. Improved confinement regimes induced by limiter biasing in the TJ-II stellarator. *Plasma Phys. Control. Fusion*, 46(1):287, 2003.

[33] I.C. Nascimento, Y.K. Kuznetsov, J.H.F. Severo, A.M.M. Fonseca, A. Elfimov, V. Bellintani, M. Machida, M.V.A.P. Heller, R.M.O. Galvão, E.K. Sanada, and J.I. Elizondo. Plasma confinement using biased electrode in the TCABR tokamak. *Nucl. Fusion*, 45(8):796–803, 2005.

[34] M. Spolaore, R. Cavazzana, L. Marrelli, L. Carraro, P. Franz, S. Spagnolo, B. Zaniol, M. Zuin, L. Cordaro, S. Dal Bello, G. De Masi, A. Ferro, C. Finotti, L. Grando, G. Grenfell, P. Innocente, O. Kudlacek, G. Marchiori, E. Martines, B. Momo, R. Paccagnella, P. Piovesan, C. Piron, M.E. Puiatti, M. Recchia, P. Scarin, C. Taliercio, N. Vianello, and L. Zanotto. H-mode achievement and edge features in RFX-mod tokamak operation. *Nucl. Fusion*, 57(11):116039, 2017.

[35] G. G. Grenfell, I. C. Nascimento, D. S. Oliveira, Z. O. Guimares-Filho, J. I. Elizondo, A. P. Reis, R. M. O. Galvo, W. A. H. Baquero, A. M. Oliveira, G. Ronchi, W. P. de S, and J. H. F. Severo. H-mode access and the role of spectral shift with electrode biasing in the TCABR tokamak. *Phys. Plasmas*, 25(7):072301, 2018.

[36] C. Alejaldre, J. Alonso, L. Almoguera, E. Ascasíbar, A. Baciero, R. Balbín, M. Blaumoser, J. Botija, B. Brañas, E. de la Cal, A. Cappa, R. Carrasco, F. Castejón, J. R Cepero, C. Cremy, J. Doncel, C. Dulya, T. Estrada, A. Fernández, M. Francés, C. Fuentes, A. García, I. García-Cortés, J. Guasp, J. Herranz, C. Hidalgo, J.A. Jiménez, I. Kirpitchev, V. Krivenski, I. Labrador, F. Lapayese, K. Likin, M. Liniers, A. López-Fraguas, A. López-Sánchez, E. de la Luna, R. Martín, A. Martínez, M. Medrano, P. Méndez, K. McCarthy, F. Medina, B. van Milligen, M. Ochando, L. Pacios, I. Pastor, M.A. Pedrosa, A. de la Peña, A. Portas, J. Qin, L. Rodríguez-Rodrigo, A. Salas, E. Sánchez, J. Sánchez, F. Tabarés, D. Tafalla, V. Tribaldos, J. Vega, B. Zurro, D. Akulina, O. I Fedyanin, S. Grebenshchicov, N. Kharchev, A. Meshcheryakov, R. Barth, G. van Dijk, H. van der Meiden, and S. Petrov. First plasmas in the TJ-II flexible heliac. *Plasma Phys. Control. Fusion*, 41:A539, 1999.

[37] P. Manz, T.T. Ribeiro, B.D. Scott, G. Birkenmeier, D. Carralero, G. Fuchert, S.H. Müller, H.W. Müller, U. Stroth, and E. Wolfrum. Origin and turbulence spreading of plasma blobs. *Phys. Plasmas*, 22:022308, 2015.

[38] Ch.P. Ritz, E.J. Powers, T.L. Rhodes, R.D. Bengtson, K.W. Gentle, Hong Lin, P.E. Phillips, A.J. Wootton, D.L. Brower, N.C. Luhmann, W.A. Peebles, P.M. Schoch, and R.L. Hickok. Advanced plasma fluctuation analysis techniques and their impact on fusion research. *Rev. Sci. Instrum.*, 59(8):1739, 1988.

[39] C. Hidalgo, M.A. Pedrosa, N. Dreval, K.J. McCarthy, L. Eliseev, M.A. Ochando, T. Estrada, I. Pastor, E. Ascasíbar, E. Calderón, A. Cappa, A.A. Chmyga, A. Fernández, B. Gonçalves, J. Hernanz, J.A. Jiménez, S.M. Khrebtov, A.D. Komarov, A.S. Kozachok, L. Krupnik, A. López-Fraguas, A. López-Sánchez, A.V. Melnikov, F. Medina, B. van Milligen, C. Silva, F. Tabarés, and D. Tafalla. Improved confinement regimes induced by limiter biasing in the TJ-II stellarator. *Plasma Phys. Control. Fusion*, 46(1):287, 2004.

[40] C. Silva, B. Goncalves, M.A. Pedrosa, C. Hidalgo, K. McCarthy, E. Calderon, J. Herranz, I. Pastor, and O. Orozco. Transport and fluctuations during electrode biasing on TJ-II. *Czechoslovak Journal of Physics*, 55(12):1589–1596, 2005.

[41] A.V. Melnikov, C. Hidalgo, L.G. Eliseev, E. Ascasibar, A.A. Chmyga, K.S. Dyabilin, I.A. Krasilnikov, V.A. Krupin, L.I. Krupnik, S.M. Khrebtov, et al. Plasma potential and turbulence dynamics in toroidal devices (survey of T-10 and TJ-II experiments). *Nuclear Fusion*, 51(8):083043, 2011.

[42] E. Ascasíbar, T. Estrada, M. Liniers, M.A. Ochando, F.L. Tabarés, D. Tafalla, J. Guasp, R. Jiménez-Gömez, F. Castejön, D. Löpez-Bruna, et al. Global Energy Confinement Studies in TJ-II NBI Plasmas. *Contributions to Plasma Physics*, 50(6-7):594–599, 2010.

[43] J.L. Velasco, J.A. Alonso, I. Calvo, and J. Arévalo. Vanishing neoclassical viscosity and physics

of the shear layer in stellarators. *Phys. Rev. Lett.*, 109(13):135003, 2012.

[44] C. Hidalgo, M. A. Pedrosa, L. García, and A. Ware. Experimental evidence of coupling between sheared-flow development and an increase in the level of turbulence in the TJ-II stellarator. *Phys. Rev. E*, 70:067402, Dec 2004.

[45] Ch. P. Ritz, Roger D. Bengtson, S. J. Levinson, and E. J. Powers. Turbulent structure in the edge plasma of the TEXT tokamak. *The Physics of Fluids*, 27(12):2956–2959, 1984.

[46] C. Hidalgo, B. Goncalves, M.A. Pedrosa, C. Silva, R. Balbın, M. Hron, A. Loarte, K. Erents, G.F. Matthews, and R. Pitts. Experimental evidence of fluctuations and flows near marginal stability and dynamical interplay between gradients and transport in the JET plasma boundary region. *Journal of Nuclear Materials*, 313-316:863 – 867, 2003.

[47] C. Hidalgo, B. Gonçalves, M.A. Pedrosa, C. Silva, R. Balbín, M. Hron, A. Loarte, K. Erents, G.F. Matthews, and R. Pitts. Experimental evidence of fluctuations and flows near marginal stability and dynamical interplay between gradients and transport in the JET plasma boundary region. *J. Nucl. Mat.*, 313-316:863, 2003.

[48] U. Losada, A. Alonso, B. Ph. van Milligen, C. Hidalgo, B. Liu, M.A. Pedrosa, C. Silva, et al. Influence of long-scale length radial electric field components on zonal flow-like structures in the TJ-II stellarator. *Plasma Phys. Control. Fusion*, 58(8):084005, 2016.

[49] D. A. Schaffner, T. A Carter, G. D. Rossi, D. S. Guice, J. E. Maggs, S. Vincena, and B. Friedman. Modification of turbulent transport with continuous variation of flow shear in the large plasma device. *Phys. Rev. Lett.*, 109(13):135002, 2012.

[50] P. Beyer, S. Benkadda, X. Garbet, and P.H. Diamond. Nondiffusive transport in tokamaks: Three-dimensional structure of bursts and the role of zonal flows. *Phys. Rev. Lett.*, 85(23):4892, 2000.

[51] S. Yi, J.M. Kwon, P.H. Diamond, and T.S. Hahm. Turbulence spreading as a non-local mechanism of global confinement degradation and ion temperature profile stiffness. *Nucl. Fusion*, 55(9):092002, 2015.

[52] Ph. Ghendrih, Y. Sarazin, G. Ciraolo, G. Darmet, X. Garbet, V. Grangirard, P. Tamain, S. Benkadda, and P. Beyer. Transport barrier fluctuations governed by SOL turbulence spreading. *J. Nucl. Mat.*, 363:581–585, 2007.